A Modeling Method to Improve Quantitation of Fluorodeoxyglucose Uptake in Heterogeneous Tumor Tissue

Hsiao-Ming Wu, Sung-Cheng Huang, Yong Choi, Carl K. Hoh and Randall A. Hawkins

Division of Nuclear Medicine and Biophysics, Department of Molecular and Medical Pharmacology, Laboratory of Structural Biology and Molecular Medicine, UCLA School of Medicine, Los Angeles, California

The standard approach for evaluating FDG-PET kinetic studies is based upon an assumption that tissue within a representative region of interest (ROI) is relatively homogeneous in terms of FDG kinetics. In neoplasms and other disease states, tissue within an ROI may be grossly heterogeneous, due to adjacent infarcted tissue and other causes. We have developed a method employing two ROIs (one over the tumor and another over a "reference region") to deal with this level of heterogeneity. **Methods:** The method is based on the regular FDG model but consists of six variable parameters (6P model) which uses the kinetics in the reference region to account for the normal tissue within the tumor ROI, so that the kinetic data only associated with the tumor can be estimated. Monte Carlo simulations and human PET FDG studies were used to analyze the performance of the 6P model. **Results:** The narrower 95% confidence intervals of parameter estimates, which centered at the true tumor rate constants, and the smaller correlation matrix of the 6P model showed the better performance of the 6P model compared to the standard "homogeneous" four-parameter FDG model. Computer simulations further showed that the 6P model can accurately estimate the microparameters (rate constants: K_1^* (ml/min/g), k_2^* (min^{-1}), k_3^* (min^{-1}), k_4^* (min^{-1})) and the macroparameter (K (ml/min/g)) of tumor cells regardless of the percent weight of tumor cells in the lesions. **Conclusions:** The new method can produce more reliable and accurate estimates of tumor glucose metabolic rates with dynamic PET FDG studies.

Key Words: FDG-PET; tumor kinetics; model; heterogeneity; quantitation

J Nucl Med 1995; 36:297–306

PET studies with 2-[^{18}F]fluoro-2-deoxy-D-glucose (FDG) are of potential utility for metabolically characterizing tumors based on kinetic characteristics and for quantifying changes in tumor metabolism before, during and after treatment. The enhanced aerobic glycolysis of malignant cells was first noted by Warburg (*1,2*). The elevated glucose utilization may be due to some combination of the increased rate of glucose transport through the cell membrane, the decreased rate of dephosphorylation and the enhanced activity of hexokinase (*3*). With an appropriate model and proper data processing, FDG-PET kinetic studies of neoplasms can produce numerical estimates of the rate constants of FDG in its capillary transport, phosphorylation and dephosphorylation.

The model currently used to analyze FDG kinetic studies of tumors is the three-compartment model originally developed by Sokoloff et al. for autoradiographic deoxyglucose studies in rat brain (3K model) (*4*). Phelps and Huang adapted the model and include a fourth rate constant to account for dephosphorylation of FDG-6-PO_4 in FDG-PET studies (4K model) (*5,6*). These models were originally designed for a localized region of tissue that is homogeneous with respect to the rate of blood flow, the transport of glucose, and the glucose and FDG concentrations in tissue. Neoplasms are, however, quite heterogeneous on the cellular level, and may also be macroscopically heterogeneous (e.g., admixture of different cell populations, such as stromal and tumor cells). As tumors grow, the relative distribution of vascular structures, stroma and necrotic tissue add complexity to the tumor FDG kinetics. Schmidt, Sokoloff et al. have previously shown that tissue heterogeneity in ROIs in brain FDG-PET studies can have significant effects on FDG model parameter values (*7*). The direct application of these "homogeneous" models (3K and 4K models) to the tumor kinetic studies can produce misleading results.

While the effect of tissue heterogeneity has been investigated for PET measurements of cerebral blood flow with ^{15}O methods, and of glucose metabolic rate with [^{18}F]FDG methods (*7–12*), an evaluation of tissue heterogeneity effect in tumor FDG studies has not been reported. Due to the lack of an appropriate model which can accurately estimate the complex kinetics in tumors, most of the FDG-PET studies in non-CNS tumors are evaluated nonkinetically using indices such as a standard uptake value (SUV)

Received Feb. 8, 1994; revision accepted Jul. 12, 1994.

For correspondence or reprints contact: Sung-Cheng Huang, DSc, Division of Nuclear Medicine & Biophysics, Department of Molecular and Medical Pharmacology, UCLA School of Medicine, 10833 Le Conte Ave., Los Angeles, CA 90024-1735.

TABLE 1
Estimation Errors of MR_{glc} Calculated 45 Minutes Following a Pulse of FDG in Different Simulated Heterogeneous Tissue* Using the 4K Model

Study no.	Source		Rate constants K_1^* (ml/min/g)	k_2^* (min^{-1})	k_3^* (min^{-1})	k_4^* (min^{-1})	MR_{glc}** error (%)
1	Rat brain†	Gray matter	0.340	0.540	0.080	0.000	27
		White matter	0.085	0.135	0.020	0.000	
2	Human brain‡	Gray matter	0.092	0.210	0.075	0.000	3.4
		White matter	0.053	0.122	0.053	0.000	
3	Melanoma§	Tumor	0.243	0.780	0.101	0.000	1.0
		Liver	0.864	0.981	0.005	0.016	
4	Melanoma§	Tumor 1	0.250	0.777	0.130	0.015	20
		Tumor 2	0.034	0.049	0.038	0.000	
5	Liver metastasis¶	Tumor 1	0.276	0.470	0.087	0.000	5.2
		Tumor 2	0.132	0.228	0.035	0.006	
6	Liver metastasis¶	Tumor 3	0.348	0.591	0.113	0.000	28
		Tumor 4	0.060	0.107	0.009	0.006	

*For each simulation study, heterogeneous tissue total activity curve was simulated using 50% of each component and a plasma input function from a human subject.

†Rate constants from Schmidt et al. (*7*)

‡Rate constants from Hawkins et al. ( )

§Unpublished data from our laboratory; liver, mean values from 10 volunteers; tumor, mean values from 25 melanoma studies; tumor 1, mean + 1 s.d. tumor 2: mean − 1 s.d.

¶Rate constants from Okazumi et al. (*15*): tumor 1: mean + 1 s.d. tumor 2: mean − 1 s.d.; tumor 3: mean + 2 s.d. tumor 4: mean − 2 s.d.

**Estimated MR_{glc} in each simulated heterogeneous tissue was calculated using the microparameters estimated by 4k model and the operational equation derived by Phelps et al. (*5*). Constant Cp and LC were assumed. True mass weighted MR_{glc} were calculated as $\overline{MR} = \Sigma_1^2 0.5MR_i$, where $MR_i = Cp/LC(K_1^*k_3^*/k_2^* + k_3^*)_i$ · % error = ((estimated MR − true $\overline{MR}$)/true $\overline{MR}$)*100%.

or a differential uptake ratio (DUR) (*13,14*). Although useful, these semiquantitative methods do not account for the kinetics of FDG transport, phosphorylation and dephosphorylation.

The potential utility of analyzing FDG model microparameters (K_1^*, k_2^*, k_3^*, and k_4^* in the 4K model) in liver tumors has been demonstrated in the literature (*15*). This study also suggested that metabolic characteristics of specific organ systems must be considered when analyzing tumor FDG kinetics. A previous study in our laboratory suggested that a three-compartment model with a vascular volume parameter fits the liver kinetics data well (*16*). The purpose of the current study is to refine the "homogeneous" compartmental model for FDG-PET kinetic studies in liver metastases and to improve the quantitative precision of tumor FDG studies by including the tissue heterogeneity effects. We developed a new method (2 ROIs, 6P FDG model) which incorporates the information in the normal liver tissue and provides the kinetic data uniquely contributed by the tumor cells in the lesions, and we have evaluated the accuracy and precision of both 4K and 6P models using data from computer simulations and tumor FDG-PET studies.

MATERIALS AND METHODS

Two ROIs and 6P FDG Model Description

In a previous study in our laboratory, we used the "homogeneous" 4K model to evaluate the heterogeneity effects in some heterogeneous tissues simulations (*17*). We found that if the differences in the rate constants between different cell groups are small, then the 4K model can accurately estimate the glucose metabolic rate, a rate approximately equal to the mass-weighted average metabolic rate of the different cell populations in the same ROI (Table 1). Based on these results, we grouped the different cells in a tumor ROI into two major cell populations. One is the tumor cell population, the other is the "reference" cell population, which contains normal cells. Each population is assumed to have a homogenous compartment behavior and has its own characteristic rate constants (K_1^* (ml/min/g), k_2^* (min^{-1}), k_3^* (min^{-1}), k_4^* (min^{-1})) for tumor cells and (K_5^* (ml/min/g), k_6^* (min^{-1}), k_7^* (min^{-1}), k_8^* (min^{-1})) for reference cells. The percent weights of the two cell populations within the ROI are w_1 and w_2, respectively (where $w_1 + w_2 = 1$). The inclusion of a fifth parameter in the 4K model improved the FDG tumor studies in our laboratory (*18,19*). Therefore the present method includes a vascular compartment with volume v_1 (% vol, or ml/100 g) (Fig. 1A).

A second ROI is drawn over a reference tissue, which contains only the normal cell population and is assumed to have the same characteristic rate constants (K_5^*, k_6^*, k_7^*, and k_8^*) as the normal cell population in the tumor ROI. The vascular compartment with volume v_2 is also included to account for the vascular space in the reference ROI (Figure 1B). Since this new method uses two ROIs and the parameter estimation procedure involves six parameters (see description of model equations), we refer to this new method as the 2 ROIs, 6 P model ("6P model").

Model Equations

According to the 6P model described above, the total amount of tracer in tumor tissue ROI, $C_{tumor}^*(t)$, is equal to the sum of

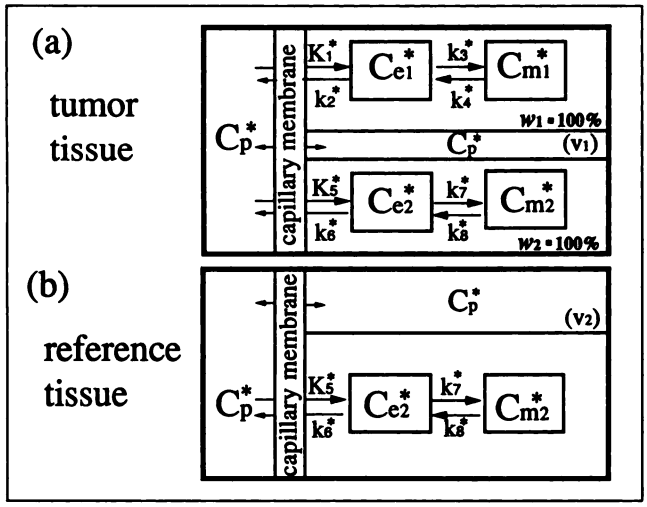

FIGURE 1. Schematic diagram of 2 ROI, 6P FDG model. Two ROIs are (A) the tumor tissue ROI and (B) reference tissue ROI. In tumor tissue ROI, two cell populations, tumor cells and reference cells, are assumed. Each occupy w_1 and w_2 of percent mass weight. $C_p^*(t)$ represents the FDG concentration in the arterial plasma, $C_e^*(t)$ and $C_m^*(t)$ represent the tissue concentrations of FDG and FDG-6-PO_4, respectively. K_1^*, k_2^*, k_3^*, k_4^* and K_5^*, k_6^*, k_7^*, k_8^*, are the first order rate constants describing the directional transport between compartments. In each ROI, a vascular compartment is included. v_1, v_2 are the vascular space volumes in tumor and reference tissue, respectively.

tracer concentrations in the tumor cell population ($C^*_{\text{tumor cell}}(t)$), the reference cell population ($C^*_{\text{ref cell}}(t)$), and the tissue blood radioactivity. The replacement of the tissue blood radioactivity with the plasma radioactivity ($C_p^*(t)$) was validated by Phelps et al. (*5*). Thus

$$C^*_{\text{tumor}}(t) = w_1 C^*_{\text{tumor cell}}(t) + w_2 C^*_{\text{ref cell}}(t) + v_1 C_p^*(t), \quad \text{Eq. 1}$$

where w_1 and w_2 are the percent mass weights of the tumor and reference cell population, respectively, and v_1 is the vascular compartment volume. The total amount of tracer in the reference tissue ROI is equal to the sum of tracers in the reference cells and in the vascular compartment:

$$C^*_{\text{ref}}(t) = C^*_{\text{ref cell}}(t) + v_2 C_p^*(t). \quad \text{Eq. 2}$$

Combining Equations 1 and 2 and rearranging, one has

$$C^*_{\text{tumor}}(t) = w_1 C^*_{\text{tumor cell}}(t) + w_2 C^*_{\text{ref}}(t) + (v_1 - w_2 v_2) C_p^*(t). \quad \text{Eq. 3}$$

Based on the regular FDG model, the rates of change in concentrations of FDG ($C_{e1}^*(t)$) and FDG-6-P ($C_{m1}^*(t)$) in the tumor cells can be expressed as:

$$\frac{d}{dt} C_{e1}^*(t) = K_1^* C_p^*(t) - (k_2^* + k_3^*) C_{e1}^*(t) + k_4^* C_{m1}^*(t), \quad \text{Eq. 4}$$

$$\frac{d}{dt} C_{m1}^*(t) = k_3^* C_{e1}^*(t) - k_4^* C_{m1}^*(t). \quad \text{Eq. 5}$$

Equations 4 and 5 can be solved in terms of $C_p^*(t)$:

$$C_{e1}^*(t) = \frac{K_1^*}{\alpha_2 - \alpha_1} [(k_4^* - \alpha_1) e^{-\alpha_1 t} + (\alpha_2 - k_4^*) e^{-\alpha_2 t}] \otimes C_p^*(t), \quad \text{Eq. 6}$$

$$C_{m1}^*(t) = \frac{K_1^* k_3^*}{\alpha_2 - \alpha_1} [(e^{-\alpha_1 t} - e^{-\alpha_2 t})] \otimes C_p^*(t), \quad \text{Eq. 7}$$

where $\otimes$ denotes the mathematical operation of convolution and

$$\alpha_1 = [k_2^* + k_3^* + k_4^* - \sqrt{(k_2^* + k_3^* + k_4^*)^2 - 4k_2^* k_4^*}]/2, \quad \text{Eq. 8}$$

$$\alpha_2 = [k_2^* + k_3^* + k_4^* + \sqrt{(k_2^* + k_3^* + k_4^*)^2 - 4k_2^* k_4^*}]/2. \quad \text{Eq. 9}$$

Since the total amount of tracer in tumor cells, $C^*_{\text{tumor cell}}(t)$, is equal to the sum of $C_{e1}^*(t)$ and $C_{m1}^*(t)$.

$$C^*_{\text{tumor cell}}(t) = C_{e1}^*(t) + C_{m1}^*(t). \quad \text{Eq. 10}$$

Substituting $C_{e1}^*(t)$ and $C_{m1}^*(t)$ from Equations 6 and 7, Equation 10 becomes:

$$C^*_{\text{tumor cell}}(t) = \frac{K_1^*}{\alpha_2 - \alpha_1} [(k_3^* + k_4^* - \alpha_1) e^{-\alpha_1 t} + (\alpha_2 - k_3^* - k_4^*) e^{-\alpha_2 t}] \otimes C_p^*(t). \quad \text{Eq. 11}$$

Since $w_1 + w_2 = 1$, combing Equations 3 and 11 and replacing $w_1 = 1 - w_2$, the total amount of tracer in tumor tissue ROI is:

$$C^*_{\text{tumor}}(t) = \frac{(1 - w_2) K_1^*}{\alpha_2 - \alpha_1} [(k_3^* + k_4^* - \alpha_1) e^{-\alpha_1 t} + (\alpha_2 - k_3^* - k_4^*) e^{-\alpha_2 t}] \otimes C_p^*(t) + w_2 C^*_{\text{ref}}(t) + (v_1 - w_2 v_2) C_p^*(t) \quad \text{Eq. 12}$$

Equation 12 is the relationship used in this study for determining the rate constants, the vascular volume, and the percent mass weight of the tumor cell population. The time-activity curve obtained from the reference tissue ROI is used directly for $C^*_{\text{ref}}(t)$ in Equation 12, which is fitted to the time-activity curve from the tumor tissue ROI with a least-squared nonlinear regression routine (*20*). The six parameters estimated in the regression procedure are: $p_1 = (1 - w_2)K_1^*$; $p_2 = k_2^*$; $p_3 = k_3^*$; $p_4 = k_4^*$; $p_5 = v_1 - w_2 v_2$; and $p_6 = w_2$.

After these six parameters are estimated, the following parameters can be calculated:

$$K_1^* = p_1/(1 - p_6), \quad \text{Eq. 13}$$

$$w_1 = 1 - p_6 \quad \text{Eq. 14}$$

The tumor metabolic rate of glucose (MR_{glc}, μmole/min/g) can then be calculated with the following equation:

$$MR_{glc} = K(Cp/LC), \quad \text{Eq. 15}$$

where the macroparameter K (ml/min/g):

$$K = K_1^* k_3^* / (k_2^* / k_3^*), \quad \text{Eq. 16}$$

C_p is the plasma glucose concentration and LC is the lumped constant (*5*). If one assumes that LC in a given tumor cell population does not change over time, then the macroparameter K in Equation 16 can be used to estimate changes in the glucose metabolic rate in tumor cells. Therefore, with a dynamic FDG-PET imaging sequence, all the microparameters (K_1^*, k_2^*, k_3^* and k_4^*), the macroparameter (K), which describe the tumor cell population FDG kinetics, and the percent mass weight of tumor cell population (w_1) in the tumor tissue ROI can be estimated by using the 2 ROIs, 6P FDG model.

Computer Simulations

The time-activity curve of each compartment in the homogeneous tumor cells ($C^*_{e1}(t)$ and $C^*_{m1}(t)$) and reference cells ($C^*_{e2}(t)$ and $C^*_{m2}(t)$) were generated using the regular FDG model (i.e., the "homogeneous" 4K model (*5*)). $C^*_{e1}(t)$ and $C^*_{m1}(t)$ were generated using Equations 6 and 7. $C^*_{e2}(t)$ and $C^*_{m2}(t)$ were generated using the following equations:

$$C^*_{e2}(t) = \frac{K^*_5}{\alpha_{22} - \alpha_{12}}[(k^*_8 - \alpha_{12})e^{-\alpha_{12}t} + (\alpha_{22} - k^*_8)e^{-\alpha_{22}t}] \otimes C^*_p(t), \quad \text{Eq. 17}$$

$$C^*_{m2}(t) = \frac{K^*_5 k^*_7}{\alpha_{22} - \alpha_{12}}[(e^{-\alpha_{12}t} - e^{-\alpha_{22}t})] \otimes C^*_p(t), \quad \text{Eq. 18}$$

where α_{12} and α_{22} are defined as Equations 8 and 9 but with the rate constants replaced by the corresponding ones for the normal cell population. The rate constants used to simulate the tumor and reference tissue time-activity curves were the average values obtained from a melanoma study conducted in our laboratory (Table 1, study no. 3). A patient's plasma time-activity curve ($C^*_p(t)$) following a bolus intravenous injection of FDG was used as the input function in the simulations.

The time course (0–50 min) of the total activity in the reference tissue ROI ($C^*_{ref}(t)$), and that of the total activity in the hypothetical tumor tissue ROI ($C^*_{tumor}(t)$) that contained different percent weights of tumor and liver cell populations (w_1 and w_2, respectively) were simulated as:

$$C^*_{ref}(t) = C^*_{e2}(t) + C^*_{m2}(t) + v_2 C^*_p(t), \quad \text{Eq. 19}$$

$$C^*_{tumor}(t) = w_1(C^*_{e1}(t) + C^*_{m1}(t)) + w_2(C^*_{e2}(t) + C^*_{m2}(t)) + v_1 C^*_p(t), \quad \text{Eq. 20}$$

where v_1 and v_2 are the vascular volumes in tumor and reference tissues, respectively. Each simulated time-activity curve was integrated over 18 time intervals with mid-scan times, T = 0.1, 0.3, 0.6, 0.9, 1.5, 2.5, 3.5, 4.5, 6, 8.5, 12.5, 17.5, 22.5, 27.5, 37.5, 42.5 and 47.5 min, which corresponded approximately to the PET scanning sequence used in routine tumor FDG studies in our laboratory.

Monte Carlo Simulation

The performance of parameter estimation by the 6P model was analyzed by Monte Carlo simulations. Poisson noise (comparable to the level in real PET studies) was also included in the simulations. (The noise levels in the last 30 min of tumor tissue, liver tissue and plasma time-activity curves were 3.2%, 3.7% and 4.5%, respectively.) Using the equations and rate constants mentioned earlier, 500 realizations of the tumor tissue total activity curves ($C^*_{tumor}(t)$) were simulated, each containing 70% tumor cells (w_1 = 0.7) and 30% normal liver cells (w_2 = 0.3), with 10% of plasma activity ($C^*_p(t)$) (v_1 = 0.1) added to each curve. Additionally, 500 realizations of the reference tissue total activity curve ($C^*_{ref}(t)$) were simulated, each containing 100% of normal cells, with 25% of plasma activity (v_2 = 0.25) added to each curve. Both 4K and 6P models were then applied to each of the 500 simulations. The 4K model in this study referred to the three-compartment FDG model by Phelps et al. (*5*), a blood volume term was included (same model configuration as Figure 1B, except with rate constants equal to K^*_1, k^*_2, k^*_3 and k^*_4). While the 6P model required both tumor and reference tissue time-activity curves, the 4K model used only the tumor tissue time-activity curve. All data simulations and parameter estimations were performed on a VAX STATION 4000 (Digital Equipment Corp., Maynard, MA) using a nonlinear regression routine written in BLD software (*20*).

To evaluate the heterogeneity effects on parameter estimates, a different set of simulations were generated using both the 4K and the 6P models. Nine tumor tissue time-activity curves were simulated, each containing 10%, 20%, 30%, 40%, 50%, 60%, 70%, 80% and 90% of tumor cells (w_1 = 0.1, 0.2, 0.3, 0.4, 0.5, 0.6, 0.7, 0.8 and 0.9, w_2 = 0.9, 0.8, 0.7, 0.6, 0.5, 0.4, 0.3, 0.2, and 0.1, correspondingly), with 10% of plasma activity (v_1 = 0.1). The reference tissue total activity curve was simulated with 100% of normal cells and 25% of plasma activity (v_2 = 0.25). One realization of each time-activity curve was simulated. Poisson noise was added in each simulation curve so that the noise levels in the last 30 min of tumor and liver tissue TACs were 3.0% ~ 4.0% and 3.7%, respectively.

Human PET FDG Studies

Since the 6P model can be readily applied if representative reference tissue is in the field of view, data from one melanoma liver metastases and two breast cancer patients were analyzed. Following intravenous injection of 10 mCi of FDG, dynamic images were obtained with a Siemens/CTI 931/08 tomograph which simultaneously acquires 15 image planes each 6.95 mm thick in a 10.8-cm axial field of view. The PET studies were performed over the liver and spleen in the melanoma patients and over the heart and the superior part of the liver in the breast cancer patients. The dynamic sequence consisted of twelve 10-sec, four 30-sec, and fourteen 240-sec scans for a total scan time of ~60 min. Cross-sectional images were reconstructed into a 128 × 128 pixel matrix using a Shepp-Logan filter with a cut-off frequency of 0.30 Nyquist frequency, yielding an in-plane spatial resolution of ~10 mm FWHM. Photon attenuation was corrected with a 20-min transmission scan using a $^{68}Ge/^{68}Ga$ external ring source. The blood samples were taken from a hand vein, heated to 44°C to arterialize the blood at 5–10-sec intervals over the first 3 min and at progressively lengthening intervals for the remainder of the study. For the melanoma study, the reference tissue ROIs were over the normal liver tissue. For the breast cancer studies, the contralateral breast (without the lesion) was chosen to define the reference tissue ROI. Time-activity curves of the tumor and reference tissue regions were then obtained from the dynamic FDG images. Both 4K and 6P models were applied to estimate the microparameters and macroparameters of the FDG kinetics.

RESULTS

Simulation

Figure 2A shows one realization of the time-activity curves generated in Monte Carlo simulations. Figure 2B shows the time-activity curves obtained from the melanoma study in a human subject. Note the similarity between the two sets of time-activity curves.

Analysis of Estimation Results

To determine if a successful fit of the data to the model has been obtained, a number of statistic parameters were examined. Table 2 summarizes the parameter estimation results of both 4K and 6P models for the Monte Carlo simulations. While the 6P model accurately estimated the tumor cell rate constants (with errors <2.5%), results from the 4K model were approximately equal to the mass-

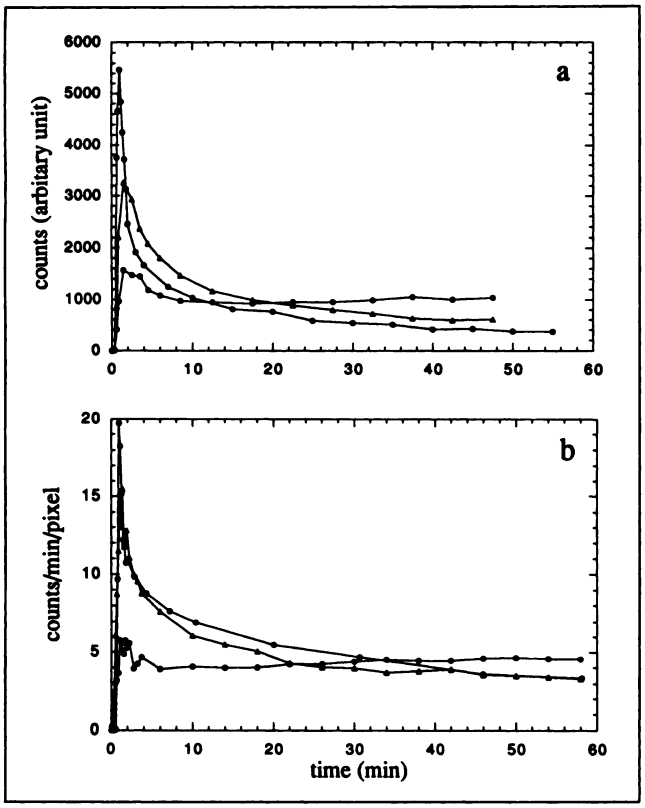

FIGURE 2. Representative time-activity curves from (A) Monte Carlo simulations with Poisson noise and (B) a melanoma patient's FDG-PET study. (open circle) plasma input functions; (solid circle) time-activity curve of tumor tissue; (open triangle) time-activity curve of reference tissue.

weighted average of the rate constants of tumor and normal cells (with errors equal to 3.3%, 3.0%, 38% and 98%, respectively).

By comparing the coefficients of variation, correlation matrixes (Table 2), sample distributions and 95% confidence interval (Fig. 3) of each parameter estimate, the performance of the 6P model is superior by all these criteria.

Effects of Tissue Heterogeneity in Parameter Estimation

Figures 4 and 5A show the microparameters (K_1^*, k_2^*, k_3^*, and k_4^*) and macroparameter (K, calculated with Equation 16) estimated from hypothetical heterogeneous tissue simulations containing different percent weights of the tumor cell population. While the 6P model's estimates remained consistent regardless of the percent weights of the tumor cell population, the 4K model's estimates varied. Although the simulations with low percent weight of the tumor cell population (w_1 = 0.1, 0.2) showed relatively large errors in the parameter estimates when the 6P model was used, the errors were mainly due to the large noise-to-signal in these cases. When noise-free time-activity curves were used, the accurate parameters were estimated by the 6P model. Figure 5B shows the correlation between true w_1's and those estimated by the 6P model. The correlation coefficient, r, was 0.9987.

Melanoma FDG Studies

Figures 6A and 6B show two image planes of a melanoma patient's FDG-PET study. The kinetic data of one lesion in each image was analyzed. ROI 1 and ROI 3 were the regular size ROIs when the 4K model was used (Fig. 6C and 6D). To test the validity of the 6P model, which assumes that tumor tissue contains both tumor and normal cell populations, ROIs (ROI 2, 4 and 5) larger than the regular size were also drawn on both images. The large ROIs were used to assess the sensitivity of the method to ROI size and reduce the statistical noise in the ROI value. Table 3 lists the microparameter and macroparameter values of both lesions as estimated by the 4K and 6P models. The microparameters estimated from the 4K model were not comparable for the two lesions (using ROIs 1 and 3), and large residuals were observed. However, the microparameters estimated by the 6P model were more consistent for the two lesions and for the different ROIs (ROI 2, 4 and 5). In addition, the 6P model fitting had smaller residuals. Although the 6P model did not always provide a significant improvement in the data fit as compared to the 4K model (F test (*21*), for ROI 2 and ROI 5, $p < 0.05$), the convergence of the regression was always better for the 6P model. The initial values in the regression were also found to be less crucial when the 6P model was used. Furthermore, as the ROI size was increased, better statistics (smaller residuals) were obtained, whereas the macroparameters, K, estimated by the 4K model were underestimated due to the inclusion of normal liver tissue.

Breast Cancer FDG Studies

Table 4 lists the microparameters and macroparameters obtained from two breast cancer FDG-PET studies. The regular size ROIs which covered the whole lesions were used. When the percent mass weight of the tumor cells was large (lesion 1, w_1 = 0.85), both 4k and 6P models provided comparable results. However, if the lesion contained less tumor cells (lesion 2, w_1 = 0.19), the macroparameter was underestimated by the 4K model due to the large fraction of normal cells. The values of the microparameters estimated by the 6P model for the two different breast lesions from two different patients were similar while they differed greatly for the 4K model.

DISCUSSION

The use of FDG-PET for qualitative and quantitative evaluation of tumor metabolism is expanding rapidly (*22*). Kinetic evaluations of tissue glucose metabolic rates can be obtained either from autoradiographic method or modeling method (*4–6*). Because the autoradiographic method requires a priori population estimates of the model rate constants which are not yet available for neoplasms outside of the CNS, it is generally not applicable for these tumors (*23*). One of the key assumptions in the deoxyglucose method (3K model, Sokoloff) is the kinetic homoge-

TABLE 2
Parameter Estimate Summary of Monte Carlo Simulations (n = 500) Using the 4K and 6P FDG Models*

4K model						6P model†					
$\hat{p}_1$	0.415	$s(\hat{p}_1)$	0.068	$CV(\hat{p}_1)$	16.4	$\hat{p}_1$	0.176	$s(\hat{p}_1)$	0.023	$CV(\hat{p}_1)$	13.2
$\hat{p}_2$	0.865	$s(\hat{p}_2)$	0.133	$CV(\hat{p}_2)$	15.3	$\hat{p}_2$	0.799	$s(\hat{p}_2)$	0.063	$CV(\hat{p}_2)$	7.9
$\hat{p}_3$	0.045	$s(\hat{p}_3)$	0.004	$CV(\hat{p}_3)$	9.2	$\hat{p}_3$	0.100	$s(\hat{p}_3)$	0.007	$CV(\hat{p}_3)$	7.0
$\hat{p}_4$	4.6E−4	$s(\hat{p}_4)$	0.002	$CV(\hat{p}_4)$	528	$\hat{p}_4$	1.3E−5	$s(\hat{p}_4)$	1.9E−5	$CV(\hat{p}_4)$	150
$\hat{p}_5$	0.102	$s(\hat{p}_5)$	0.029	$CV(\hat{p}_5)$	28.4	$\hat{p}_5$	0.031	$s(\hat{p}_5)$	0.035	$CV(\hat{p}_5)$	113
						$\hat{p}_6$	0.291	$s(\hat{p}_6)$	0.043	$CV(\hat{p}_6)$	14.9

Parameter correlation matrix:

	p_1	p_2	p_3	p_4	p_5
p_1	1	0.97	−0.12	0.28	−0.91
p_2	0.97	1	0.06	0.35	−0.83
p_3	−0.12	0.06	1	0.69	0.31
p_4	0.28	0.35	0.69	1	−0.20
p_5	−0.91	−0.83	0.31	−0.20	1

	p_1	p_2	p_3	p_4	p_5	p_6
p_1	1	0.83	−0.82	0.06	0.11	−0.53
p_2	0.83	1	−0.48	−0.12	−0.06	−0.24
p_3	−0.82	−0.48	1	−0.17	−0.14	0.53
p_4	0.06	−0.12	−0.17	1	−0.003	−0.06
p_5	0.11	−0.06	−0.14	−0.003	1	−0.86
p_6	−0.53	−0.24	0.53	−0.06	−0.86	1

*True values used in the simulations: $p_1(K_1^*) = 0.243$, $p_2(k_2^*) = 0.780$, $p_3(k_3^*) = 0.101$, $p_4(k_4^*) = 0$, $p_5(4K) = 0.1$, $p_5(6P) = 0.025$, $p_6(6P) = 0.3$; true mass-weighted average value: $\overline{K_1^*} = 0.429$, $\overline{k_2^*} = 0.840$, $\overline{k_3^*} = 0.0722$, $\overline{k_4^*} = 0.0048$.

†In 6P model, $p_1 = K_1^*(1 - p_5)$. Therefore, K_1^* was calculated after the fitting: $\hat{K}_1^* = 0.248$; $s(\hat{K}_1^*) = 0.028$; $CV(\hat{K}_1^*) = 11.22$.

$\hat{p}$ = mean; $s(\hat{p})$ = standard deviation; $CV(\hat{p})$ = coefficient of variation.

neity in tissue. Direct extrapolations of the method to the heterogeneous tumor systems may lead to confusing and inconsistent results.

In a recent report on the effects of tissue heterogeneity on the FDG model, Schmidt et al. demonstrated that the glucose metabolic rate could be overestimated by the 4K model due to tissue heterogeneity alone (*7*). Tissue heterogeneity is one of the key issues in tumor studies; thus, refinements of the FDG model for tumor systems are thus necessary (*23*). Although the heterogeneous model (TH model) proposed by Schmidt et al. is a more realistic representation of heterogeneous tissue (*7*), its application in specific systems, such as tumor systems, needs to be evaluated. Three major considerations are: (1) the phosphatase activity (equivalent to k_4^* in 4K model) was found in some tumor systems (*15,22,23*); (2) the exponential approximation of effective rate constants $k_2^*(t)$, and $k_3^*(t)$ and the constant ratio assumption of $k_2^*(t)/k_3^*(t)$ may not be valid in the tumor systems; and (3) the computational burden of including the heterogeneity effect. In this study, we proposed a simple model-based method to address this heterogeneity problem. As shown in Table 1, the 4K model could accurately estimate the mass weighted glucose metabolic rate of different cells in an ROI if the rate constants among these cell populations are similar. Therefore, as far as the total glucose metabolic rate is concerned, it is reasonable to group the different tumor cells as a single population by assuming that their FDG uptake kinetics are not too different. Therefore, by including both tumor and normal cell population in the formulation, the 6P model can account for the tissue heterogeneity effect due to the inclusion of background activity in the lesion ROI. This, plus the inclusion of the percent mass weighting factors (w_1 and w_2, where w_1 was replaced with $1 - w_2$) in the fitting equation (Equation 12), allowed an estimation of the rate constants characteristic of the tumor cells alone. The 6P model assumes that the FDG uptake kinetic of the normal cells in the tumor region is the same as in the reference region. If they are not the same, the error caused by the use of the 6P model should be small as long as they are not too different. However, if they are drastically different and the background is closer to the tumor kinetic, the results from the 6P model should be similar to those from the regular 4K model. More quantitative evaluation of the effects of using inaccurate reference tissue regions is needed.

Better performance of the 6P model compared to the 4K model is demonstrated by the 6P model's narrower 95% confidence regions, which centered at the true tumor cells rate constants (Fig. 3), and smaller correlation matrix (i.e., the largest correlation coefficients of 6P model is 0.86, compared to the largest correlation coefficient of 0.97 for the 4K model (Table 2)).

While the values of the microparameters and macroparameters estimated by the 4K model varied when different proportions of tumor cells were included in the tumor tissue, those estimated by the 6P model remained consistent (Fig. 4). Although parameters estimated by the 6P model still contained some errors, these errors were mainly due to the Poisson noise added in the simulation. More accurate and precise measurements of microparameters are expected to improve the quantification of tumor metabolism with PET. If a lesion contains a relatively large amount of normal cells (or cells with kinetics markedly different than tumor cells), then glucose metabolism estimated with the 4K model will be too low (Fig. 5A). With the 6P model, the macroparameter of the tumor cell population can be esti-

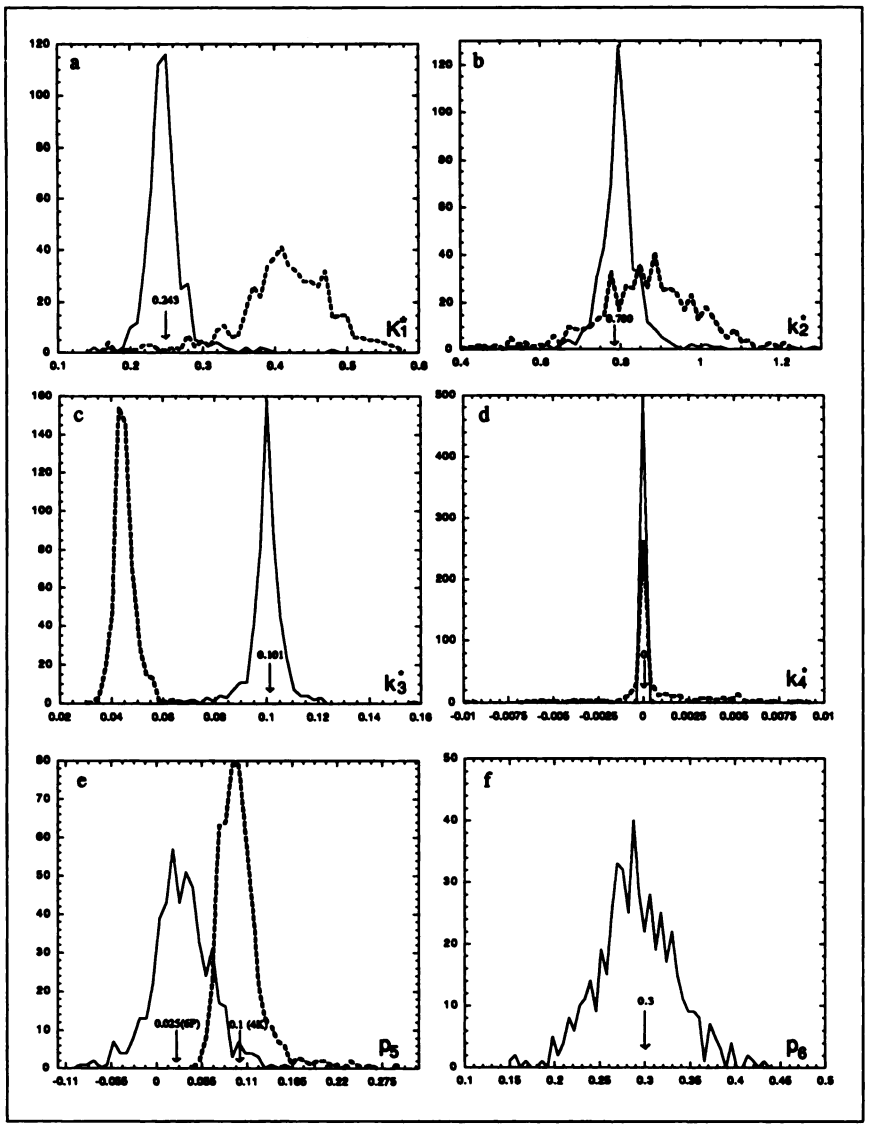

FIGURE 3. Sample distribution of estimated parameter values (y axis: no. of realizations, x axis: value of estimates) in Monte Carlo simulations (dot lines: estimates from 4K model, solid line: estimates from 6P model). The arrow in each plot points at the true value of tumor cell. The 95% confidence regions of parameter estimates are (a) K_1^* (4K model: 0.225 ~ 0.540, 6P model: 0.202 ~ 0.295 ml/min/g) (b) k_2^* (4K model: 0.553 ~ 1.110, 6P model: 0.687 ~ 0.914 min^{-1}) (c) k_3^* (4K model: 0.038 ~ 0.053, 6P model: 0.087 ~ 0.114 min^{-1}) (d) k_4^* (4K model: -5.4×10^{-3} ~ 6.4×10^{-3}, 6P model: $7.1 \times 10^{-6} \sim 1.19 \times 10^{-5}$ min^{-1}) (e) p_5 (4K model: 0.064 ~ 0.176, 6P model: −0.045% ~ 0.106% vol) (f) p_6 (mass weight of tumor cells, 6P model: 0.209 ~ 0.375).

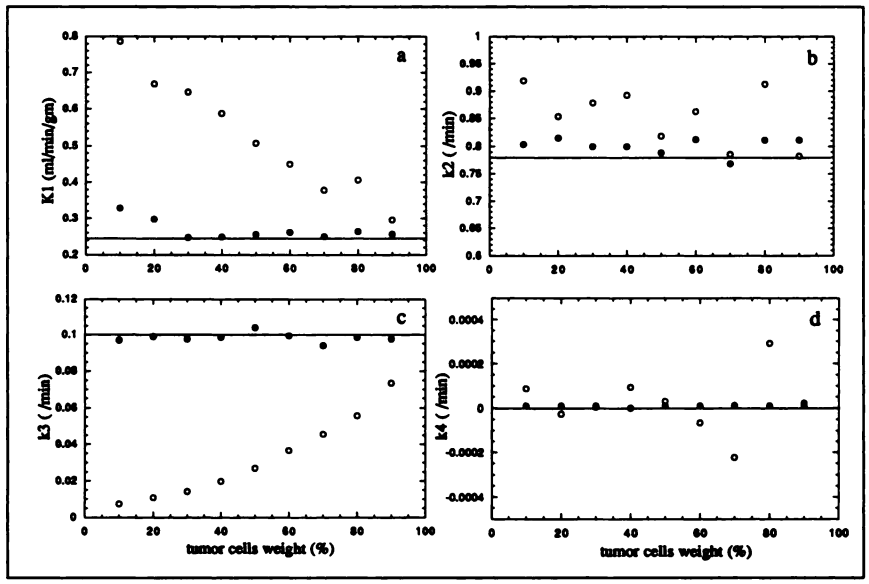

FIGURE 4. Microparameters (A) K_1^*, (B) k_2^*, (C) k_3^* and (D) k_4^*, estimated from simulated heterogeneous tissue time-activity curves containing different percent mass weights of tumor cells. (open circle): 4K model; (solid circle): 6P model. The horizontal solid line in each plot presents the true microparameter value, K_1^*, k_2^*, k_3^*, and k_4^*, of the tumor cells, respectively.

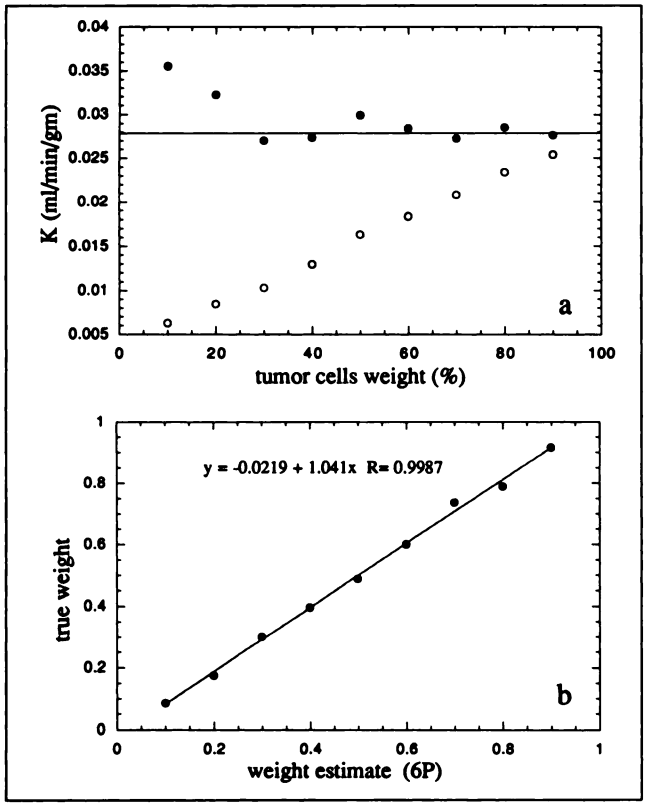

FIGURE 5. (A) Macroparameters, K, estimated from simulated heterogeneous tissue time-activity curves containing different weights of tumor cells. (open circle): 4K model; (solid circle): 6P model. The horizontal solid line in the plot presents the true macroparameter value, K, of the tumor cells. (B) Correlation of true and estimated tumor cell weights from simulated heterogeneous tissue time-activity curves containing different weights of tumor cells.

mated more directly. If one assumes a constant LC and the plasma glucose concentration is measured, the glucose metabolic rate of tumor cell population can then be obtained. Therefore, an improved differentiation between normal and malignant tissues should result from the use of the 6P model.

Another feature of the 6P model is the identifiability of the percent mass weighting factors (w_1 and w_2). These weighting factors become unidentifiable only when tumor and normal cells have very similar rate constants. In this case, the tissue is close to homogeneous, and the 4K model is applicable. Our simulations using melanoma and liver cells rate constants resulted in a good correlation of the estimated and the true percent weights (r = 0.9987). The percent mass weight of the tumor cells in the lesion can potentially provide information on the cell number changes as the tumor grows in time.

The third feature of the 6P model is its generality and feasibility. Because the 6P model does not make any assumption between the ratio of $k_2^*(t)/k_3^*(t)$, the model can be applied to heterogeneous tissues regardless of the relationship between the rate constants. Except for the requirement of a second ROI, the computation time of the 6P model is similar to that of the 4K model.

Unlike simulation data, various error sources, including the finite resolution of PET, the various sizes of lesions, the inaccurate definition of ROIs, and different levels of noise, can affect the accuracy and reliability of the estimation results. The microparameters estimated from the melanoma patients using conventional ROIs and 4K model were less reliable (Table 3, ROI 1 and ROI 3). The regression results varied with different initial values; however, by using the 6P model, some of the problems were reduced with the use of a much larger ROI (e.g., ROI 2 of Fig. 6) resulting in more reasonable parameter estimates and better statistics. Although the 6P model did not always provide a significant improvement in the fitting of lesion 2, the microparameters obtained from the 6P model were more reasonable and closer to those obtained from lesion 1. Therefore, the 6P model is less sensitive to the ROI size and noise, and can thus minimize the partial volume effects due to the small size of the lesions. Furthermore, as the ROI size is increased, (comparing the sum of squares of ROIs 3, 4 and 5 in Table 3), better statistics are expected. We expected this feature to allow one to evaluate the glucose utilization rate of tumor cells even as the lesion changes in size more accurately. Thus, the 6P model can potentially be used to give more reliable results in follow up studies.

The 2 ROIs, 6P model was originally designed for liver melanoma tumor studies. The results obtained from the breast cancer studies (Table 4) further confirmed that the 2 ROIs, 6P model can be readily applied to tumor systems to account for tissue heterogeneity when a representative reference tissue ROI is available.

The present method does not take necrotic tissue in the lesion into account. However, it has been shown that ne-

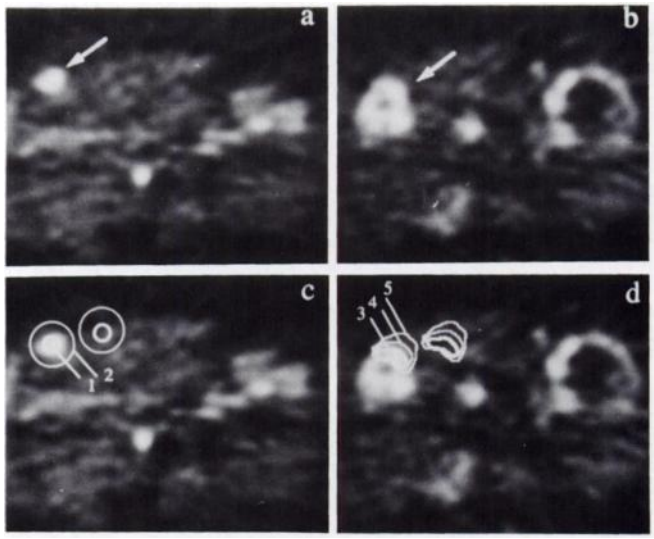

FIGURE 6. Images of liver metastases from a FDG PET melanoma study. Arrows point to (A) lesion 1 on plane 8 and (B) lesion 2 on plane 12. ROIs 1–5 on (C, D) were the tumor ROIs, the unlabeled ROIs were the corresponding reference ROIs for 6P model with same sizes and shapes. ROI size: ROI 1 (2.3 cm^2), ROI 2 (16 cm^2), ROI 3 (6.0 cm^2), ROI 4 (7.1 cm^2), and ROI 5 (10.3 cm^2).

TABLE 3
Microparameters and Macroparameters Obtained from Melanoma Patient with Liver Metastasis

	4K model					6P model			
	Lesion 1	Lesion 2				Lesion 1	Lesion 2		
	ROI 1	ROI 3	ROI 4	ROI 5		ROI 2	ROI 3	ROI 4	ROI 5
K_1^* (ml/min/g)	0.024	0.303	0.107	0.092	K_1^* (ml/min/g)	0.053	0.089	0.067	0.056
k_2^* (min^{-1})	1E−04	1.374	0.462	0.417	k_2^* (min^{-1})	0.195	0.230	0.162	0.068
k_3^* (min^{-1})	0.085	0.155	0.156	0.135	k_3^* (min^{-1})	0.226	0.163	0.245	0.127
k_4^* (min^{-1})	0.005	4E−05	2E−05	6E−04	k_4^* (min^{-1})	0.041	2E−04	0.012	0.012
K (ml/min/g)	0.024	0.031	0.027	0.022	K (ml/min/g)	0.028	0.037	0.040	0.036
					w_1	0.605	0.807	0.722	0.617
ss	30.2	14.8	11.7	7.08	ss	1.8	14.0	10.4	5.5

ss = sum of squares.

TABLE 4
Microparameters and Macroparameters Obtained from Breast Cancer Patients

	4K model			6P model	
	Lesion 1	Lesion 2		Lesion 1	Lesion 2
K_1^* (ml/min/g)	0.050	0.060	K_1^* (ml/min/g)	0.060	0.059
k_2^* (min^{-1})	0.219	0.207	k_2^* (min^{-1})	0.281	0.268
k_3^* (min^{-1})	0.078	0.006	k_3^* (min^{-1})	0.075	0.035
k_4^* (min^{-1})	0.002	5E−05	k_4^* (min^{-1})	6E−04	0.000
K (ml/min/g)	0.013	0.002	K (ml/min/g)	0.013	0.004
			w_1	0.85	0.19
ss	10.4	1.3	ss	10.0	1.2

ss = sum of squares.

crotic areas do not accumulate FDG (*24*). The inclusion of necrotic tissue into ROIs was avoided in the present study.

CONCLUSION

In this study we show that the 2 ROIs and 6P FDG model can be readily applied to tumor systems to account for tissue heterogeneity in tumors when a representative "reference" tissue region is available. Furthermore, the new method can correct the partial volume effect, is less sensitive to the tumor and ROI sizes, and allows larger ROIs be drawn to improve noise statistics. Thus, the new method can potentially produce more reliable and accurate estimates of tumor glucose metabolic rates with dynamic PET-FDG studies.

ACKNOWLEDGMENTS

The authors thank the UCLA cyclotron staff for synthesizing the FDG compound used in this study; Mr. Ron Sumida and the UCLA PET scanner staff for performing the PET studies; and Drs. E. J. Hoffman, M. Dahlbom, A. R. Ricci, K. Gardner and D. Truong for instrumentation, computer hardware, and software support. This work was partly supported by Department of Energy contract DE-AC0376-SF00012 and National Institutes of Health grant RO1CA56655.

REFERENCES

1. Warburg O. *The metabolism of tumors.* London: Constable and Co.; 1930.
2. Warburg O. On the origin of cancer cells. *Science* 1956;123:309–314.
3. Weber G. Enzymology of cancer cells. *N Engl J Med* 1977;296:541–551.
4. Sokoloff L, Reivich M, Kennedy C, et al. The [^{14}C] deoxyglucose method for the measurement of local cerebral glucose utilization: theory, procedure and normal values in the conscious and anesthetized albino rat. *J Neurochem* 1977;28:897–916.
5. Phelps ME, Huang SC, Hoffman EJ, Selin CJ, Sokoloff L, Kuhl DE. Tomographic measurement of local cerebral glucose metabolic rate in humans with (F-18) 2-fluoro-2-deoxy-D-glucose: validation of method. *Ann Neurol* 1979;6:371–388.
6. Huang SC, Phelps ME, Hoffman EJ, Sideris K, Selin CJ, Kuhl DE. Noninvasive determination of local cerebral metabolic rate of glucose in man. *Am J Physiol* 1980;238:E69–E82.
7. Schmidt K, Mies G, Sokoloff L. Model of kinetic behavior of deoxyglucose in heterogeneous tissue in brain: a reinterpretation of the significance of parameters fitted to homogeneous tissue models. *J Cereb Blood Flow Metab* 1991;11:10–24.
8. Baron JC, Frackowiak RSJ, Herholz K, et al. Use of PET methods for measurement of cerebral energy metabolism and hemodynamics in cerebrovascular disease. *J Cereb Blood Flow Metab* 1989;9:723–742.
9. Huang SC, Mahoney DK, Phelps ME. Quantification in positron emission tomography. 8. Effects of nonlinear parameter estimation on functional images. *J Comput Assist Tomogr* 1987;11:314–325.
10. Herholz K, Patlak CS. The influence of tissue heterogeneity on results of fitting nonlinear model equations to regional tracer uptake curves: with an application to compartmental models used in positron emission tomography. *J Cereb Blood Flow Metab* 1987;7:214–229.
11. Schmidt K, Lucignani G, Moresco RM, et al. Errors introduced by tissue heterogeneity in estimation of local cerebral glucose utilization with current

kinetic models of the [^{18}F]fluorodeoxyglucose method. *J Cereb Blood Flow Metab* 1992;12:823–834.
12. Lucignani G, Schmidt KC, Moresco RM, et al. Measurement of regional cerebral glucose utilization with fluorine-18-FDG and PET in heterogeneous tissues: theoretical considerations and practical procedure. *J Nucl Med* 1993;34:360–369.
13. Haberkorn U, Strauss LC, Dimitrakopoulou A, et al. PET studies of fluorodeoxyglucose metabolism in patients with recurrent colorectal tumors receiving radiotherapy. *J Nucl Med* 1991;32:1485–1490.
14. Adler LP, Blair HF, Makley JT. Noninvasive grading of musculoskeletal tumors using PET. *J Nucl Med* 1991;32:1058–1512.
15. Okazumi S, Isono K, Enomoto K, et al. Evaluation of liver tumors using ^{18}F-fluorodeoxyglucose PET: characterization of tumor and assessment of effect of treatment. *J Nucl Med* 1992;33:333–339.
16. Choi Y, Hawkins RA, Huang SC, et al. An evaluation of the effect of glucose ingestion and kinetic model configurations of FDG in the normal liver. *J Nucl Med* 1994;35: in press.
17. Wu C, Huang SC, Choi Y, Hawkins RA. Effects of tissue heterogeneity (TH) on FDG parameter estimates [Abstract]. *J Nucl Med* 1993;34:40p.
18. Hawkins RA, Phelps ME, Huang SC. Effects of temporal sampling, glucose metabolic rates and disruptions of the blood-brain barrier on the FDG model with and without a vascular compartment: studies in human brain tumors with PET. *J Cereb Blood Flow Metab* 1986;6:170–183.
19. Messa C, Choi Y, Hoh CK, et al. Quantification of glucose utilization in liver metastases: parametric imaging of FDG uptake with PET. *J Comput Assist Tomogr* 1992;16:684–689.
20. Carson RE, Huang SC, Phelps ME. BLD: a software system for physiological data handling and model analysis. *Proceedings of the fifth annual symposium on computer applications in medical care.* 1981:562–565.
21. Landaw EM, DiStefano JJ, III. Multiexponential, multicompartmental, and noncompartmental modeling. II. Data analysis and statistical considerations. *Am J Physiol* 1984;246:R665–R677.
22. Fischman AJ, Alpert NM. FDG-PET in oncology: there's more to it than looking at pictures [Editorial]. *J Nucl Med* 1993;34:6–11.
23. Hawkins RA, Choi Y, Huang SC, Messa C, Hoh CK, Phelps ME. Quantitating tumor glucose metabolism with FDG and PET [Editorial]. *J Nucl Med* 1992;33:339–344.
24. Paul R, Johansson R, Kellokumpu-Lehtinen PL, Söderström KO, Kangas L. Tumor localization with ^{18}F-2-fluoro-2-deoxy-D-glucose: comparative autoradiography, glucose 6-phosphatase histochemistry, and histology of renally implanted sarcoma of the rat. *Res Exp Med* 1985;185:87–94.